ChemComm

COMMUNICATION

View Article Online
View Journal

Cite this: DOI: 10.1039/c5cc04808g

Received 10th June 2015,
Accepted 30th June 2015

DOI: 10.1039/c5cc04808g

www.rsc.org/chemcomm

A MOF platform for incorporation of complementary organic motifs for CO_2 binding†

Pravas Deria,‡[a] Song Li,‡[b] Hongda Zhang,[b] Randall Q. Snurr,*[b] Joseph T. Hupp*[a] and Omar K. Farha*[ac]

CO_2 capture is essential for reducing the carbon footprint of coal-fired power plants. Here we show, both experimentally and computationally, a new design strategy for capturing CO_2 in nanoporous adsorbents. The approach involves 'complementary organic motifs' (COMs), which have a precise alignment of charge densities that is complementary to the CO_2 quadrupole. Two promising COMs were post-synthetically incorporated into a robust metal–organic framework (MOF) material using solvent-assisted ligand incorporation (SALI). We demonstrate that these COM-functionalized MOFs exhibit high capacity and selectivity for CO_2 relative to other reported motifs.

In the coming decades, carbon capture and sequestration (CCS) could play a significant role in reducing the greenhouse gas emissions that arise from burning fossil fuels.[1,2] For existing coal-fired power plants, the major cost of CCS is separating CO_2 from the other components of the flue gas. Many studies have, therefore, focused on developing viable strategies to separate CO_2 from N_2, which is the main component of flue gas streams exiting from coal-fired power plants. Amine scrubbing[2] is the most well developed technology, but there is a high energy cost to regenerate the aqueous amine solutions. Many researchers have studied porous adsorbent materials such as activated carbons and zeolites as more energy-efficient alternatives.[3,4] However, the difficulty in precise tailoring of their structures has made it challenging to optimize these porous materials for carbon sequestration.

Metal–organic frameworks (MOFs) are a class of crystalline porous materials consisting of multitopic organic linkers and metal-based nodes.[5–8] The chemical diversity of MOFs, along with their typically high accessible surface area,[8] has rendered MOFs promising candidates for a wide range of applications including gas capture, separation, and storage.[9–15] The modular chemistry of these materials enables one to fine tune their pore structures during synthesis. Furthermore, MOFs are amenable to various post-synthesis manipulations to incorporate desired chemical moieties into nanoscale pores.[16–19]

In the context of CCS, MOFs[11,14,20] with various chemical functionalities[21] have been investigated; the majority of these consist of Lewis basic moieties (*i.e.* $-NH_2$,[22–26] –OH,[27,28] –SH[29] *etc.*) or ionic or dipolar X–F moieties[15,30–34] (X = C,[15,33,34] P,[31] and Si[30,32]) that interact with the Lewis acidic C atom of the CO_2 molecule.

MOF structures containing Lewis acidic moieties, *e.g.* coordinatively unsaturated metal sites that bind CO_2 *via* one of its oxygen atoms, also may exhibit good selectivity for CO_2.[14,36] A sophisticated strategy that uses two precisely positioned, Lewis acidic metal centres was introduced by Li *et al.*[35] and called a 'single-molecule trap' (SMT) (Scheme 1a). We reasoned that it should be possible to design organic groups that can function similarly to the metal-based SMTs by positioning functional groups that bind the various atoms of a CO_2 molecule. Organic functionalities should be more easily incorporated into MOFs and can be designed with a wide diversity of modular functionalities with the potential for improved selectivity toward CO_2. In this study, we propose organic motifs (Scheme 1c and d) featuring partial charges ($\delta^+\cdots\delta^-\cdots\delta^+$) precisely positioned *via* polar organic functionalities to complement the quadrupolar charge distribution in O═C═O (Scheme 1b). We demonstrate that, with proper design, such COMs can be readily incorporated into MOFs and can exhibit high selectivity for CO_2 over N_2.

We tested two COMs: a small *N*-α-fluorenylmethyloxycarbonyl (FMoc)-protected triglycine peptide (*i.e.* **F3G-H**) and a 2,6-diacetylaminopyridine moiety (*i.e.* **DAP-H**). Both have appropriate arrangements of hydrogen atoms (–NH) and either oxygen (–CO) or pyridine nitrogen (Scheme 1c and d) atoms that are complementary to the charge distribution in CO_2. **F3G-H** is a commercially available tripeptide and was chosen because it exhibits torsional flexibility due to the absence of side chains in its backbone.

[a] *Department of Chemistry, Northwestern University, 2145 Sheridan Road, Evanston, Illinois 60208, USA. E-mail: j-hupp@northwestern.edu, o-farha@northwestern.edu*
[b] *Department of Chemical and Biological Engineering, Northwestern University, 2145 Sheridan Road, Evanston, Illinois 60208, USA. E-mail: snurr@northwestern.edu*
[c] *Department of Chemistry, Faculty of Science, King Abdulaziz University, Jeddah, Saudi Arabia*

† Electronic supplementary information (ESI) available: Procedures, materials, and instrumentation; characterization (N_2 adsorption, BET, NMR spectra, and DRIFTS) of **SALI-n**; simulation details. See DOI: 10.1039/c5cc04808g

‡ These authors contributed equally.

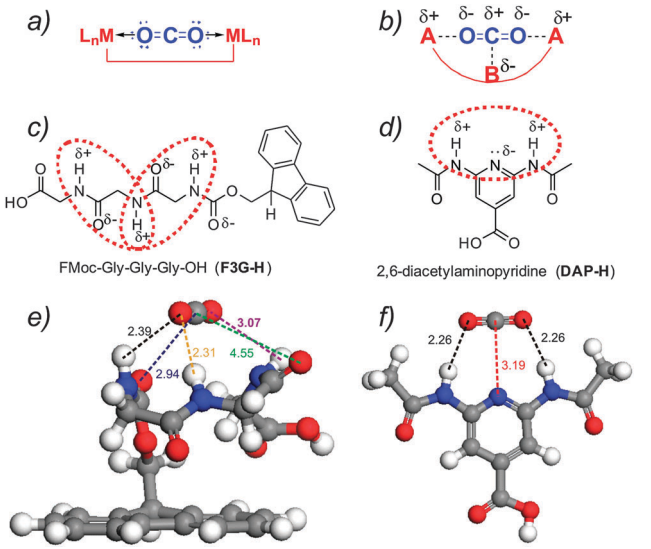

Scheme 1 Schematic representations of (a) SMT designed for CO_2 molecules involving two coordinatively unsaturated metal sites[35] and (b) COM involving precise alignment of charge densities complementary to the CO_2 quadrupole by positioning alternating Lewis acid (A) and Lewis base (B) sites. Design of COMs with amide functionalities in (c) *N*-α-fluorenylmethyloxycarbonyl (FMoc) protected triglycine (**F3G-H**) and (d) 2,6-diacetylaminopyridine-4-carboxylic acid (DAP-H). (e) and (f) CO_2 binding with COMs as predicted by DFT computations.

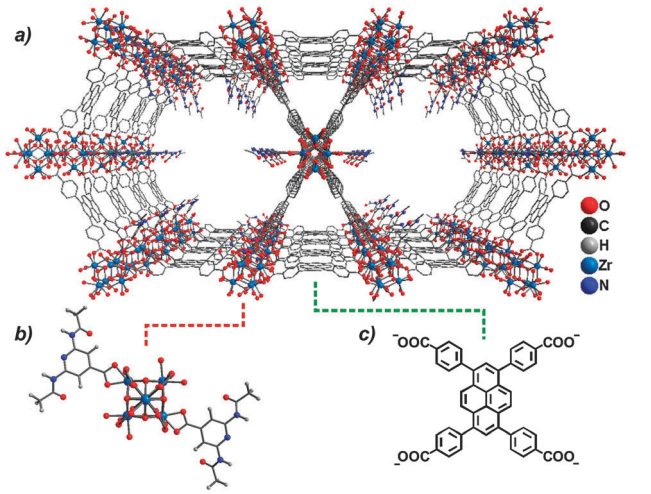

Fig. 1 SALI, a heterogenization strategy for carboxylic acid-derived functional groups[37,38] applied to the MOF **NU-1000**: (a) molecular representation of SALI-derived **SALI-DAP** (along the *c*-axis; H-atoms of the framework were removed for clarity); (b) the corresponding functionalized node;[39] and (c) the linker of **NU-1000**.

DAP-H provides a more rigid comparison. It was not clear *a priori* if flexibility or rigidity would better promote CO_2 binding and selectivity over N_2. One can imagine that rigidity, if it corresponds to optimal host pre-organization, would be preferred, but if the COM is not optimally pre-organized, then low-energy-cost flexibility would be a desirable feature.

Quantum mechanical calculations (geometries calculated with density functional theory (DFT) and energies calculated at the MP2 level; see ESI,† Section S6) revealed that the flexible **F3G-H** moiety adopts a tertiary structure that creates the COM for CO_2 involving the amide –NH proton and –CO oxygen (Scheme 1e). The shortest –NH···O=C=O distance is predicted to be 2.39 Å, and the corresponding distance between the **F3G-H** carbonyl oxygen and the carbon of CO_2 is 2.94 Å. The predicted binding energy (MP2) is −27 kJ mol^{-1}. The more rigid **DAP** moiety has previously been investigated as a H-bond donor–acceptor–donor motif[40] and possesses an alternating charge distribution that is also complementary to the quadrupolar CO_2 molecule (Scheme 1d). Quantum mechanical calculations (DFT geometries and MP2 energies) reveal a significant binding energy (−17 kJ mol^{-1}) with a shorter NH···O=C=O distance (2.26 Å) (Scheme 1f) than that observed with **F3G-H**. A negligible change in O–C–O angle and the essentially unaltered O–C bond length in these COM-bound CO_2 molecules suggest that the interaction is electrostatic in nature (see Table S3 and Fig. S15 in ESI,† Section S6).[41]

In this study, we used the $[Zr_6(\mu_3\text{-}O)_4(\mu_3\text{-}OH)_4(\text{-}OH)_4(\text{-}OH_2)_4]^{8+}$ node of the MOF **NU-1000** [molecular formula $Zr_6(\mu_3\text{-}O)_4(\mu_3\text{-}OH)_4(\text{-}OH)_4(\text{-}OH_2)_4(TBAPy)_2$] (see Fig. 1, Fig. S2 and S12, ESI;† H_4TBAPy is 1,3,6,8-tetrakis(*p*-benzoic acid)pyrene)[42,43] as a platform for Solvent-Assisted Ligand Incorporation (SALI),[37,38,44] to heterogenize a **F3G** or **DAP** moiety within the mesoporous MOF channels. Previous studies[17,37,38,44] have established that SALI (a) relies on Zr(IV)-carboxylate bond formation on the **NU-1000** node to incorporate chemical moieties, (b) provides a platform to evaluate the performance of new chemical functionalities in a porous solid environment without the need to prepare a new MOF linker containing the chemical functionality of interest, and (c) enhances chemical[44] and water vapor[45] stability.

Microcrystalline **NU-1000**[42] material, upon exposure to a 0.03 M solution of **F3G-H** or **DAP-H** in a DMSO : MeCN solvent mixture, yielded **SALI-F3G** or **SALI-DAP**. ^{1}H NMR data of digested samples (in 10% D_2SO_4/DMSO-d_6) revealed incorporation of **F3G** or **DAP** in the **NU-1000** channels (4 **F3G** or 2 **DAP** moieties per node; see ESI,† Section S3B for detailed synthesis and characterization data). The N_2 adsorption data at 77 K for the **SALI-F3G** and **SALI-DAP** samples (Fig. S5, ESI†) revealed retention of type IVc isotherms from the parent compound with Brunauer–Emmett–Teller (BET) surface areas of 890 and 1225 m^2 g^{-1}, pore volumes of 0.54 and 0.84 cm^3 g^{-1} and Barrett–Joyner–Halenda (BJH) pore diameters of 29 and 29.5 Å respectively. (Note, for the parent **NU-1000**, these metrics are 2145 m^2 g^{-1}, 1.46 cc g^{-1}, and 31 Å, respectively.)

Both the **SALI-F3G** and **SALI-DAP** samples show Langmuir type CO_2 adsorption isotherms at 273–293 K (Fig. 2a and Fig. S8, ESI†), with uptake of 1.65 mmol g^{-1} (37 cm^3 g^{-1}) and 2.29 mmol g^{-1} (50 cm^3 g^{-1}), respectively, at 1 bar and 273 K (uptake for the parent **NU-1000**[37] was 2.86 mmol g^{-1} or 64 cm^3 g^{-1}; note a 35% higher gravimetric uptake for **SALI-DAP** over **SALI-F3G**). These values, when corrected for the difference in molar mass of the functionalized materials, exhibit similar volumetric uptakes of ~30.5 cm^3 cm^{-3} for all three samples (see Fig. S8, ESI†). Both of the SALI-derived samples, however, entailed a slightly steeper CO_2 uptake in the CO_2 adsorption profiles at low pressure, resulting in higher volumetric uptake (Fig. S8, ESI†) at lower pressure

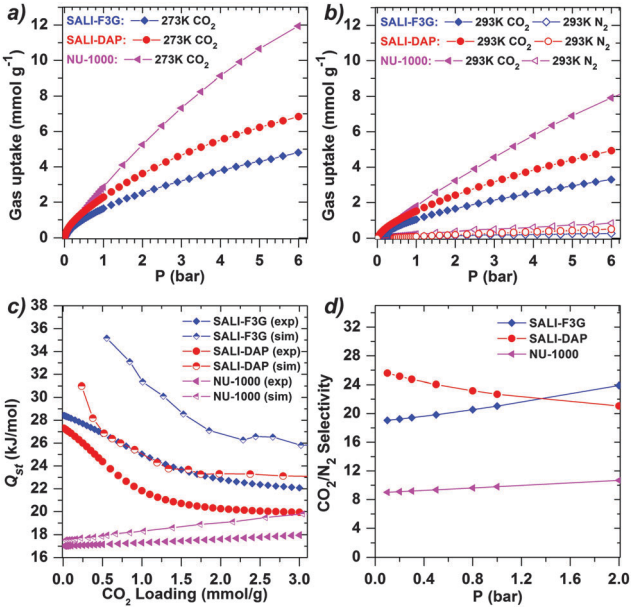

Fig. 2 (a and b) Experimental CO_2 and N_2 adsorption isotherms for **SALI-F3G**, **SALI-DAP**, **NU-1000** samples at specified temperatures. (c) Q_{st} for CO_2 from experimental isotherms and from GCMC simulations (T_{sim} = 273 K). (d) The IAST selectivity of CO_2 over N_2 (15 : 85) from fitting of the corresponding experimental isotherms (T = 293 K) for **SALI-F3G**, **SALI-DAP**, and **NU-1000** samples.

(~0.2 bar) relative to the unmodified **NU-1000**. The higher CO_2 uptake for **SALI-DAP** compared to **SALI-F3G** above 1 bar and their similar uptake below 1 bar are consistent with the behavior predicted by grand canonical Monte Carlo (GCMC) simulation, (Fig. S13, ESI;† T = 273–293 K).

The average binding energy of CO_2 in the MOF samples was estimated by analyzing isotherms collected at multiple temperatures. A dual-site Langmuir model fitting followed by Clausius–Clapeyron analysis (see ESI,† Section S5) of the experimental data provided the loading-dependent isosteric heat of adsorption (Q_{st}) plot shown in Fig. 2c. As qualitatively predicted by the GCMC simulations, at the zero-loading limit (Q_{st}^0), the **SALI-F3G** and **SALI-DAP** samples show higher values (~27–28 kJ mol^{-1}) than the parent **NU-1000** (~17 kJ mol^{-1}). At higher loadings, the Q_{st} plot for **SALI-F3G** plateaus around 23 kJ mol^{-1} at a loading of ~1.7 mmol g^{-1}, whereas for **SALI-DAP**, the plateau is ~20 kJ mol^{-1} at a loading of ~1.5 mmol g^{-1}. The GCMC results suggest that we can assign these values to adsorption at weaker binding sites, *i.e.* sites remaining after saturating primary sites at loadings of ~1.5 and ~2 CO_2 per **F3G** and **DAP** functional groups. Note that the bulky FMoc protecting group can facilitate CO_2 adsorption *via* conventional pore confinement,[33,35,37] thus contributing to the overall Q_{st} value.

Differences in the degree of the pore confinement effect and the strength of interaction between CO_2 and the primary binding sites should be reflected in differences in selectivity for CO_2 over N_2. With this in mind, we used ideal adsorbed solution theory (IAST), together with single-component adsorption isotherms (experiments), to estimate selectivities.[46] As shown in Fig. 2d, for a CO_2 : N_2 feed ratio of 15 : 85, the selectivity at low pressure was found to be ~26 for **SALI-DAP**, ~19 for **SALI-F3G**, and ~9 for unmodified **NU-1000**.[37] Thus **SALI-DAP** promises to exhibit greater selectivity than not only **SALI-F3G**, but also Lewis-acid-based "single molecule traps."[35] Working capacities of these samples for flue gas composition were estimated from the single component CO_2 isotherms recorded at 293 K: for example, the gravimetric working capacities at VSA condition[47] can be ranked as **SALI-DAP** > **NU-1000** > **SALI-F3G** (Table S5, ESI†).

To justify whether the improved Q_{st}^0 values in **SALI-DAP** and **SALI-F3G** are indeed mainly due to the selective binding of CO_2 with the COMs, we designed two control samples that do not bear a COM or COM-forming functionality. With comparable physical parameters (Fig. S16 and S17 and Table S4, ESI†) relative to the COM-derived **SALI-F3G** and **SALI-DAP**, these control samples **SALI-F2A** (F2A = Fmoc protected dialanine) and **SALI-OAB** (OAB = *o*-aminobenzoate) exhibit significantly lower Q_{st}^0 values (Fig. S18, ESI†). The Q_{st} values eventually plateau at *ca.* 22 kJ mol^{-1}, an energy associated with the 'secondary' binding sites in these functionalized **NU-1000** materials.

Fig. 3 shows snapshots from GCMC simulations for CO_2 adsorption at various loadings. Compared to the parent **NU-1000** material, **SALI-F3G** and **SALI-DAP** adsorb larger numbers of CO_2 molecules near the MOF nodes where the functional groups are located. In addition to engaging in specific interactions of CO_2, the added functional groups help define confined spaces that indirectly facilitate CO_2 uptake—behavior that is reminiscent of what has been reported recently for perfluoroalkane-tailored versions of **NU-1000**.[37]

In summary, with the help of computational modelling, we have designed and experimentally studied two 'complementary organic motifs', **F3G-H** and **DAP-H**, with precise alignment of charge densities complementary to the CO_2 quadrupole, for CO_2 capture and separation. Incorporation of the designed COMs into MOFs was facilitated by SALI, which simplifies

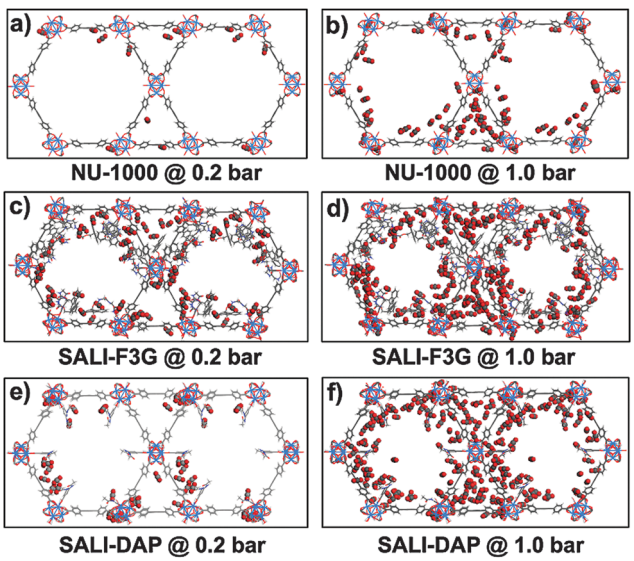

Fig. 3 Snapshots of CO_2 adsorption from GCMC simulations at various pressures for (a and b) **NU-1000**, (c and d) **SALI-F3G**, and (e and f) **SALI-DAP** (T = 273 K).

synthesis procedures relative to more conventional node and/or linker based approaches. We find that COMs when incorporated in MOFs can function as primary CO_2 binding sites, thereby enhancing Q_{st} values. The enhanced heats of adsorption and the enhanced CO_2 adsorption of the MOFs with integrated COMs are in good qualitative agreement with GCMC simulations, lending further credibility to the value of simulations for understanding and even predicting adsorption behavior. The findings reported here highlight the potential of synergistic theoretical design and experimental study to identify and develop new organic functionalities for CO_2 capture and separation. We are optimistic that these approaches, including the facile synthesis strategy, can be usefully extended to related problems in carbon capture and chemical separations.

JTH and RQS gratefully acknowledge support from the Global Climate and Energy Project. OKF gratefully acknowledges funding from the Army Research Office (project number W911NF-13-1-0229). Computations were in part performed at the National Energy Research Scientific Computing Center, which is supported by the Office of Science of the U.S. Department of Energy under Contract No. DE-AC02-05CH11231. This research was also supported in part through the computational resources and staff contributions provided for the Quest high performance computing facility at Northwestern University.

Notes and references

1 D. W. Keith, *Science*, 2009, **325**, 1654–1655.
2 G. T. Rochelle, *Science*, 2009, **325**, 1652–1654.
3 S. Choi, J. H. Drese and C. W. Jones, *ChemSusChem*, 2009, **2**, 796–854.
4 J. Wang, L. Huang, R. Yang, Z. Zhang, J. Wu, Y. Gao, Q. Wang, D. O'Hareb and Z. Zhong, *Energy Environ. Sci.*, 2014, **7**, 3478–3518.
5 O. M. Yaghi, M. O'Keefe, N. W. Ockwig, H. K. Chae, M. Eddaoudi and J. Kim, *Nature*, 2003, **423**, 705–714.
6 S. Horike, S. Shimomura and S. Kitagawa, *Nat. Chem.*, 2009, **1**, 695–704.
7 M. O'Keeffe and O. M. Yaghi, *Chem. Rev.*, 2012, **112**, 675–702.
8 O. K. Farha, I. Eryazici, N. C. Jeong, B. G. Hauser, C. E. Wilmer, A. A. Sarjeant, R. Q. Snurr, S. T. Nguyen, A. Ö. Yazaydın and J. T. Hupp, *J. Am. Chem. Soc.*, 2012, **134**, 15016–15021.
9 O. K. Farha, A. Ö. Yazaydın, I. Eryazici, C. D. Malliakas, B. G. Hauser, M. G. Kanatzidis, S. T. Nguyen, R. Q. Snurr and J. T. Hupp, *Nat. Chem.*, 2010, **2**, 944–948.
10 R. B. Getman, Y.-S. Bae, C. E. Wilmer and R. Q. Snurr, *Chem. Rev.*, 2012, **112**, 703–723.
11 J.-R. Li, J. Sculley and H.-C. Zhou, *Chem. Rev.*, 2012, **112**, 869–932.
12 Y. Peng, V. Krungleviciute, I. Eryazici, J. T. Hupp, O. K. Farha and T. Yildirim, *J. Am. Chem. Soc.*, 2013, **135**, 11887–11894.
13 M. P. Suh, H. J. Park, T. K. Prasad and D.-W. Lim, *Chem. Rev.*, 2012, **112**, 782–835.
14 K. Sumida, D. L. Rogow, J. A. Mason, T. M. McDonald, E. D. Bloch, Z. R. Herm, T.-H. Bae and J. R. Long, *Chem. Rev.*, 2012, **112**, 724–781.
15 C. E. Wilmer, O. K. Farha, Y.-S. Bae, J. T. Hupp and R. Q. Snurr, *Energy Environ. Sci.*, 2012, **5**, 9849–9856.
16 S. M. Cohen, *Chem. Rev.*, 2012, **112**, 970–1000.
17 P. Deria, J. E. Mondloch, O. Karagiaridi, W. Bury, O. K. Farha and J. T. Hupp, *Chem. Soc. Rev.*, 2014, **43**, 5896–5912.
18 M. Lalonde, W. Bury, O. Karagiaridi, Z. Brown, J. T. Hupp and O. K. Farha, *J. Mater. Chem. A*, 2013, **1**, 5453–5468.
19 O. Karagiaridi, W. Bury, J. E. Mondloch, J. T. Hupp and O. K. Farha, *Angew. Chem., Int. Ed.*, 2014, **53**, 4530–4540.
20 J. Liu, P. K. Thallapally, B. P. McGrail, D. R. Brown and J. Liu, *Chem. Soc. Rev.*, 2012, **41**, 2308–2322.
21 V. Colombo, C. Montoro, A. Maspero, G. Palmisano, N. Masciocchi, S. Galli, E. Barea and J. A. R. Navarro, *J. Am. Chem. Soc.*, 2012, **134**, 12830–12843.
22 T. M. McDonald, D. M. D'Alessandro, R. Krishna and J. R. Long, *Chem. Sci.*, 2011, **2**, 2022–2028.
23 T. M. McDonald, W. R. Lee, J. A. Mason, B. M. Wiers, C. S. Hong and J. R. Long, *J. Am. Chem. Soc.*, 2012, **134**, 7056–7065.
24 X. Wang, H. Li and X.-J. Hou, *J. Phys. Chem. C*, 2012, **116**, 19814–19821.
25 R. Vaidhyanathan, S. S. Iremonger, G. K. H. Shimizu, P. G. Boyd, S. Alavi and T. K. Woo, *Science*, 2010, **330**, 650–653.
26 R. Vaidhyanathan, S. S. Iremonger, G. K. H. Shimizu, P. G. Boyd, S. Alavi and T. K. Woo, *Angew. Chem., Int. Ed.*, 2012, **51**, 1826–1829.
27 D. Rankine, A. Avellaneda, M. R. Hill, C. J. Doonan and C. J. Sumby, *Chem. Commun.*, 2012, **48**, 10328–10330.
28 Z. Chen, S. Xiang, H. D. Arman, P. Li, S. Tidrow, D. Zhao and B. Chen, *Eur. J. Inorg. Chem.*, 2010, 3745–3749.
29 K.-K. Yee, N. Reimer, J. Liu, S.-Y. Cheng, S.-M. Yiu, J. Weber, N. Stock and Z. Xu, *J. Am. Chem. Soc.*, 2013, **135**, 7795–7798.
30 P. Kanoo, S. K. Reddy, G. Kumari, R. Haldar, C. Narayana, S. Balasubramanian and T. K. Maji, *Chem. Commun.*, 2012, **48**, 8487–8489.
31 S.-i. Noro, Y. Hijikata, M. Inukai, T. Fukushima, S. Horike, M. Higuchi, S. Kitagawa, T. Akutagawa and T. Nakamura, *Inorg. Chem.*, 2013, **52**, 280–285.
32 P. Nugent, Y. Belmabkhout, S. D. Burd, A. J. Cairns, R. Luebke, K. Forrest, T. Pham, S. Ma, B. Space, L. Wojtas, M. Eddaoudi and M. J. Zaworotko, *Nature*, 2013, **495**, 80–84.
33 D.-X. Xue, A. J. Cairns, Y. Belmabkhout, L. Wojtas, Y. Liu, M. H. Alkordi and M. Eddaoudi, *J. Am. Chem. Soc.*, 2013, **135**, 7660–7667.
34 C. A. Fernandez, P. K. Thallapally, R. K. Motkuri, S. K. Nune, J. C. Sumrak, J. Tian and J. Liu, *Cryst. Growth Des.*, 2010, **10**, 1037–1039.
35 J.-R. Li, J. Yu, W. Lu, J. Sculley, P. B. Balbuena and H.-C. Zhou, *Nat. Commun.*, 2013, **4**, 1538.
36 Y.-S. Bae, B. G. Hauser, O. K. Farha, J. T. Hupp and R. Q. Snurr, *Microporous Mesoporous Mater.*, 2011, **141**, 231–235.
37 P. Deria, J. E. Mondloch, E. Tylianakis, P. Ghosh, W. Bury, R. Q. Snurr, J. T. Hupp and O. K. Farha, *J. Am. Chem. Soc.*, 2013, **135**, 16801–16804.
38 P. Deria, W. Bury, J. T. Hupp and O. K. Farha, *Chem. Commun.*, 2014, **50**, 1965–1968.
39 Note that a maximum of 2 DAPs per node was incorporated instead of a complete 4 per node stoichiometry.
40 A. Llanes-Pallas, C.-A. Palma, L. Piot, A. Belbakra, A. Listorti, M. Prato, P. Samorì, N. Armaroli and D. Bonifazi, *J. Am. Chem. Soc.*, 2009, **131**, 509–520.
41 W. L. Queen, M. R. Hudson, E. D. Bloch, J. A. Mason, M. I. Gonzalez, J. S. Lee, D. Gygi, J. D. Howe, K. Lee, T. A. Darwish, M. James, V. K. Peterson, S. J. Teat, B. Smit, J. B. Neaton, J. R. Long and C. M. Brown, *Chem. Sci.*, 2014, **5**, 4569–4581.
42 J. E. Mondloch, W. Bury, D. Fairen-Jimenez, S. Kwon, E. J. DeMarco, M. H. Weston, A. A. Sarjeant, S. T. Nguyen, P. C. Stair, R. Q. Snurr, O. K. Farha and J. T. Hupp, *J. Am. Chem. Soc.*, 2013, **135**, 10294–10297.
43 N. Planas, J. E. Mondloch, S. Tussupbayev, J. Borycz, C. J. Cramer, J. T. Hupp, O. K. Farha and L. Gagliardi, *J. Phys. Chem. Lett.*, 2014, **5**, 3716–3723.
44 P. Deria, W. Bury, I. Hod, C.-W. Kung, O. Karagiaridi, J. T. Hupp and O. K. Farha, *Inorg. Chem.*, 2015, **54**, 2185–2192.
45 P. Deria, Y. G. Chung, R. Q. Snurr, J. T. Hupp and O. K. Farha, *Chem. Sci.*, 2015, DOI: 10.1039/c1035sc01784j.
46 A. L. Myers and J. M. Prausnitz, *AlChE J.*, 1965, **11**, 121–127.
47 G. Srinivas, V. Krungleviciute, Z.-X. Guo and T. Yildirim, *Energy Environ. Sci.*, 2014, **7**, 335–342.

